Journal of the Korean Electrochemical Society
Vol. 25, No. 1, 2022, 32-41
https://doi.org/10.5229/JKES.2022.25.1.32

Research Paper
pISSN 1229-1935
eISSN 2288-9000

Improvement of Electrochemical Performance of Lithium-ion Secondary Batteries using Double-Layered Thick Cathode Electrodes

Isheunesu Phiri[1†], Jeong-Tae Kim[1†], Ssendagire Kennedy[1†], Muchakayala Ravi[1,2], Yong Min Lee[3]**, and Myung-Hyun Ryou[1]*

[1]*Department of Chemical and Biological Engineering, Hanbat National University, 125 Dongseo-daero, Yuseong-gu, Daejeon, 34158, Republic of Korea*
[2]*Department of Science & Humanities, N.B.K.R.I.S.T, Vidyanagar-524413, Andhra Pradesh, India*
[3]*Department of Energy Science and Engineering, Daegu Gyeongbuk Institute of Science and Technology (DGIST), 333 Techno Jungang-daero, Hyeonpung-eup, Dalseong-gun, Daegu 42988, Republic of Korea*

(Received December 27, 2020 : Revised February 5, 2022 : Accepted February 14, 2022)

ABSTRACT : Various steps in the electrode production process, such as slurry mixing, slurry coating, drying, and calendaring, directly affect the quality and, consequently, mechanical properties and electrochemical performance of electrodes. Herein, a new method of slurry coating is developed: Double-coated electrode. Contrary to single-coated electrode, the cathode is prepared by double coating, wherein each coat is of half the total loading mass of the single-coated electrode. Each coat is dried and calendared. It is found that the double-coated electrode possesses more uniform pore distribution and higher electrode density and allows lesser extent of particle segregation than the single-coated electrode. Consequently, the double-coated electrode exhibits higher adhesion strength (74.7 N m^{-1}) than the single-coated electrode (57.8 N m^{-1}). Moreover, the double-coated electrode exhibits lower electric resistance (0.152 Ω cm^{-2}) than the single-coated electrode (0.177 Ω cm^{-2}). Compared to the single-coated electrode, the double-coated electrode displays higher electrochemical performance by exhibiting better rate capability, especially at higher C rates, and higher long-term cycling performance. Despite its simplicity, the proposed method allows effective electrode preparation by facilitating high electrochemical performance and is applicable for the large-scale production of high-energy-density electrodes.

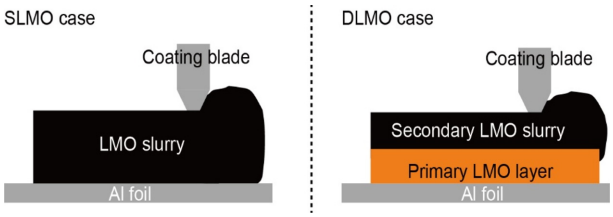

Keywords: Double coating, Segregation, Migration, Pore distribution, Conductivity

1. Introduction

Rechargeable lithium-ion batteries (LIBs) have played a crucial role in the development of portable electronic devices because of their excellent properties such as higher energy and power density, wider operating voltage range, and lower self-discharge characteristics than those of other battery systems [1-3]. Recently, concerns about environmental problems caused by carbon dioxide emission and fossil fuel depletion have expedited the commercial growth of high-energy-density batteries for use in applications such as electric vehicles (EVs) and energy storage systems (ESSs). To meet this requirement, conventional

† Corresponding authors equality contributed to this work.
*E-mail: mhryou@hanbat.ac.kr (M.-H. Ryou),
yongmin.lee@dgist.ac.kr (Y.M. Lee)

LIBs have been widely used; they are now accepted in automobile industries. Nevertheless, substantial improvement in the performance and energy density of the existing LIBs is necessary to satisfy the requirements of EVs and ESSs.

Various strategies have been developed toward the improvement in the energy density of battery systems such as development of new active materials with high energy density such as Li $Ni_{0.8}Mn_{0.1}Co_{0.1}$ [4-6], change in battery designs [7], and modification of manufacturing methods [8,9]. Among these, the development of new battery components and alternative design require considerable efforts and compromises on battery stability. In contrast, increasing the electrode thickness has been considered as a practical and promising approach to achieve high-energy-density LIBs [10-12].

A typical cathode for LIBs contains four components: the active material, conductive carbon additives e.g. Super P, polymeric binders e.g. polyvinylidene fluoride (PVDF), and Al current collectors [1-3]. Cathodes are fabricated by coating an aqueous or non-aqueous cathode slurry containing the active material, conductive carbon additives, and polymeric binders on Al current collectors. Thicker electrodes require a thicker wet slurry coating layer having a substantially larger amount of solvent than thinner electrodes. Although increasing the drying temperature is a straightforward way to accelerate solvent evaporation, this method deteriorates the electrode properties as it allows particle segregation [13] due to phase separation caused by capillary forces. Consequently, low-density electrode additives such as polymeric binders and conductive carbon additives accumulate at the top surface of the electrode and are degraded at the current collector–electrode interface [14,15]. The extent of particle segregation is proportional to the capillary path length [16-18]. Segregation affects the particle arrangement and pore structure in the electrodes, decreasing the electrochemical performance of LIBs [10,32-34]. Additionally, the calendaring process directly influences

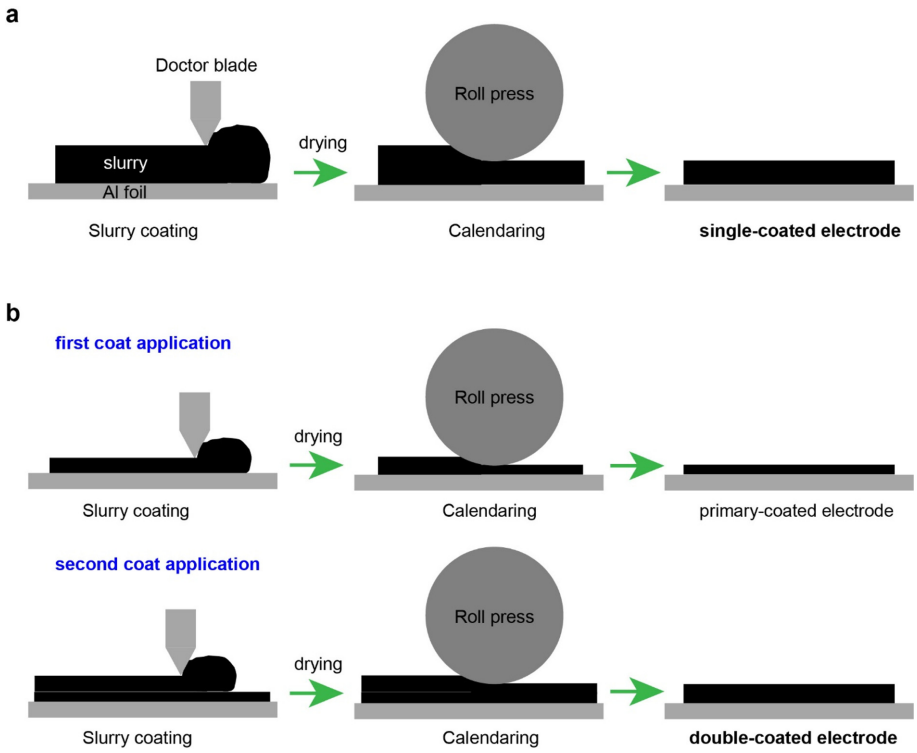

Fig. 1. Schematic of the electrode fabrication process for (a) SLMO and (b) DLMO.

the density and homogeneity of electrode composites. The inherent nonuniformity induced by the process of powder compacting becomes more severe as the film thickness increases [19,20]. Consequently, thicker electrodes have an increased risk of nonuniformity, which may cause deterioration of electrode quality after calendaring.

Many efforts have been devoted toward the development of thick electrodes composed of multiple layers with different electrode components [16,21-23]. LIBs comprising multilayered cathodes, with different proportions of electrode components in each layer, exhibit high electrochemical performance. However, the use of thicker electrodes with composition identical to that of commercial high-performance LIBs is considered the most promising and practical approach for realizing high-energy-density LIBs for EVs and ESSs.

In this study, we investigated the tap density, physical uniformity, and electrochemical properties of thick double-layered cathodes. We compared the performance of single-layered and double-layered cathodes containing the same amount of the active material (Fig. 1). The single-layered electrodes were prepared by coating the electrode slurry on Al foil once, followed by drying and calendaring (Fig. 1a). Double-layered electrodes were prepared in two steps (Fig. 1b). (i) The electrode slurry was coated on Al foil, dried, and calendared to fabricate an electrode containing half the mass loading of the single-layered electrodes. The electrodes fabricated in this step were called the primary coated electrodes. (ii) Subsequently, the electrode slurry was coated again on the primary coated electrodes, followed by drying and calendaring, to fabricate double-layered electrodes. The process was controlled to ensure that the single-layered and double-layered electrodes had the same mass loading. The morphological properties, composition, adhesion properties, and electrochemical performance of single-layered and double-layered electrodes were investigated through field emission scanning electron microscopy (FE-SEM) coupled with energy-dispersive X-ray spectroscopy (EDXS) and by using a surface and interfacial cutting analysis system (SAICAS) and battery cyclers.

2. Experimental

2.1. Materials

Lithium manganese oxide ($LiMn_2O_4$, LMO, Iljin Materials, Republic of Korea), conductive carbon (Super–P Li, Imerys, Switzerland), polyvinylidene fluoride (PVdF; KF–1300, M*w* = 350 000, Kureha, Japan), *N*–methyl–2–pyrrolidone (NMP, Sigma Aldrich Co., Ltd., Anhydrous, 99.5%, USA), aluminum foil (15 μm, Sam–A Aluminum, South Korea), polyethylene (PE) separators (ND420, Asahi Kasei E–materials, Japan, thickness = 20 μm), Li metal foil (thickness = 200 μm, Honjo Metal Co., Ltd., Japan) were used as received without further purification. A mixture of 1.15 M Li hexafluorophosphate ($LiPF_6$) in ethylene carbonate (EC)/ethyl methyl carbonate (EMC) (3/7 by volume) was purchased (Enchem Co., Ltd., South Korea) and used as an electrolyte without further purification.

2.2. Electrode preparation

Single-layered and double-layered LMO electrodes were prepared by a simple slurry coating method using a doctor blade. A homogeneous slurry was prepared by ball mixing commercial LMO active powder (94 wt.%), conductive carbon (Super P, 3 wt.%), and a polyvinylidene fluoride binder (PVDF, 3 wt.%) with NMP as a dispersing agent. To prepare the single-layered LMO (SLMO) electrode, the slurry was cast onto the Al foil current collector using a doctor blade, followed by drying in a convection oven at 130°C for 3 h. Subsequently, the electrode was roll pressed by using a gap-control roll-pressing machine (CLP–2025H, CIS, South Korea). The gap was controlled to be 60% of the initial cathode thickness. For the double-layered LMO (DLMO) electrode, the first coat was applied using half the amount of slurry by adjusting the doctor blade gap, followed by drying (130°C for 3 h) and calendaring. The second coating was applied with the remaining slurry mass, followed by drying (130°C for 3 h) and calendaring. In both coatings, the calendaring gap was controlled to be 60% of the initial cathode thickness. The prepared SLMO and DLMO were cut into discs (diameter = 12 mm) and further dried at 60°C for 12 h under vacuum before being transferred into an Ar-filled glove

box for cell assembly. The total mass loading for SLMO and DLMO was controlled to be ~14 mg cm^{-2}, while the electrode densities for SLMO and DLMO were 1.9 and 2.3 g cm^{-3}, respectively.

2.3. Electrode characterization

The morphological and compositional analysis of SLMO and DLMO electrodes were examined using a field emission scanning electron microscope (FE–SEM, JSM–6390, JEOL, Japan) equipped with an energy-dispersive X-ray spectroscopy (EDX) detector (GENESIS XM2, EDAX Inc., USA). To prepare a specimen for cross-sectional images, each SLMO and DLMO were cut using an Ar–ion milling system (E3500, Hitachi, Japan) at a constant power of 2.1 W (6 kV and 0.35 mA) under a vacuum level of $< 2.0 \times 10^{-4}$ Pa. The electric resistance R_{el} of the electrodes was determined by a four-point probe CMT-SR1000N Resistivity Measurement System (Advanced Instrument Technology).

2.4. Cell assembly and electrochemical performance

To evaluate the electrochemical performance of prepared SLMO and DLMO cathodes, 2032–type coin cells (SLMO or DLMO/Li metal) were assembled in an Ar–filled glove box. After cell assembly, cells were aged for 12 h at room temperature (25°C) and precycled, comprising of cell formation and stabilization cycles. Cell formation was done at C/10 (0.154 mA cm^{-2}) for both charging and discharging in constant current (CC) mode for 1 cycle, followed by cell stabilization step where charged at C/5 (0.308 mA cm^{-2}) in CC/constant voltage (CV) mode and discharged at C/5 (0.308 mA cm^{-2}) in CC mode for 3 cycles using a charge/discharge battery cycler (PNE Solutions, Korea). For rate capability evaluation, cells were charged at a constant rate of C/2 (0.77 mA cm^{-2}) in CC/CV mode, while discharged at various C–rates ranging from C/2 to 20 C (discharging rate sequence = C/2, 1C, 3C, 5C, 7C, 10C, 15C, 20C, and C/2). Five cycles were conducted for each discharging rate step. Cycle performance of coin cells was evaluated by charging at C/2 in CC/CV mode, while discharging at 1C in CC mode for 700 cycles. For both rate capability and cycle performance evaluation, operating voltage range and temperature were controlled in the range of 3.0 – 4.4 V and 25°C.

3. Results and Discussion

The morphological, structural, and elemental anal-

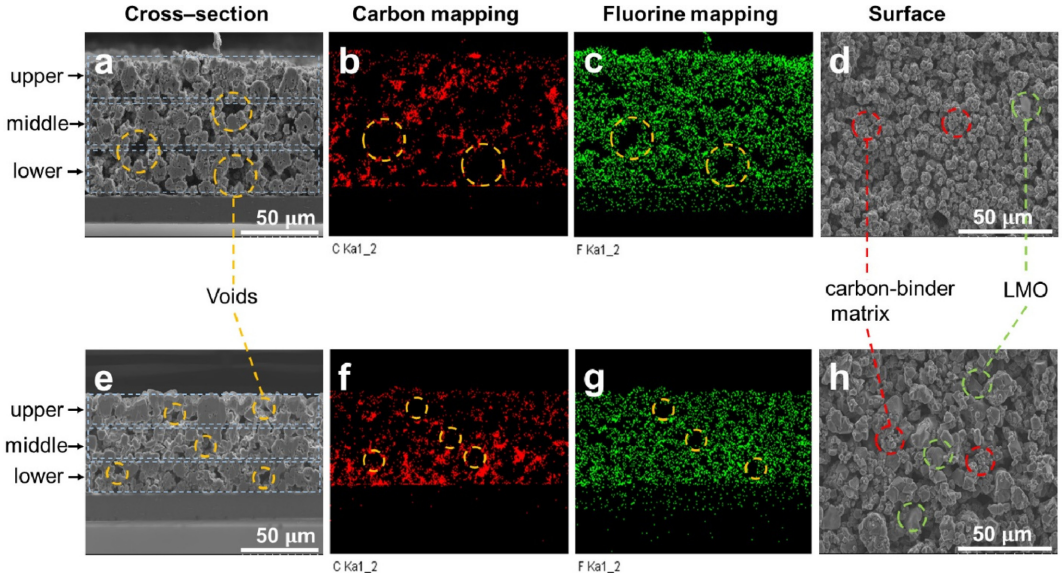

Fig. 2. SEM images and EDXS results showing the cross-section, C and F mapping profiles, and surface morphology of (a–d) SLMO and (e–h) DLMO.

yses of the electrodes were conducted through SEM and EDXS (Fig. 2). As shown in the cross-sectional SEM images (Fig. 2a), SLMO had large and irregular pore cavities that were more concentrated in the middle to lower regions of the electrode, making the electrode thick (~85 μm) and porous. In comparison, DLMO had more regular and smaller pore cavities throughout the composites, making the electrode denser and thinner (~65 μm; Fig. 2e).

PVDF polymeric binders contain carbon (C) and fluorine (F), whereas conductive carbon contains only C. Therefore, comparing the elemental mapping images of C and F could elucidate the distribution of polymeric binders and conductive carbon in the electrodes. SLMO possessed low C density near the Al substrate and in the lower region of the electrode, whereas DLMO showed high C density in that region (Fig. 2b, 2f). In contrast, SLMO displayed high C density in the upper region of the electrode, whereas DLMO showed low C density in that region. Furthermore, the SLMO surface was covered with F, which indicated the presence of a "blanket" of polymeric binders over the surface (Fig. 2c). In contrast, DLMO showed a uniform distribution of polymeric binders over the entire area of the electrode (Fig. 2g). Thus, we confirmed that the method of electrode preparation had a profound effect on the electrode microstructure.

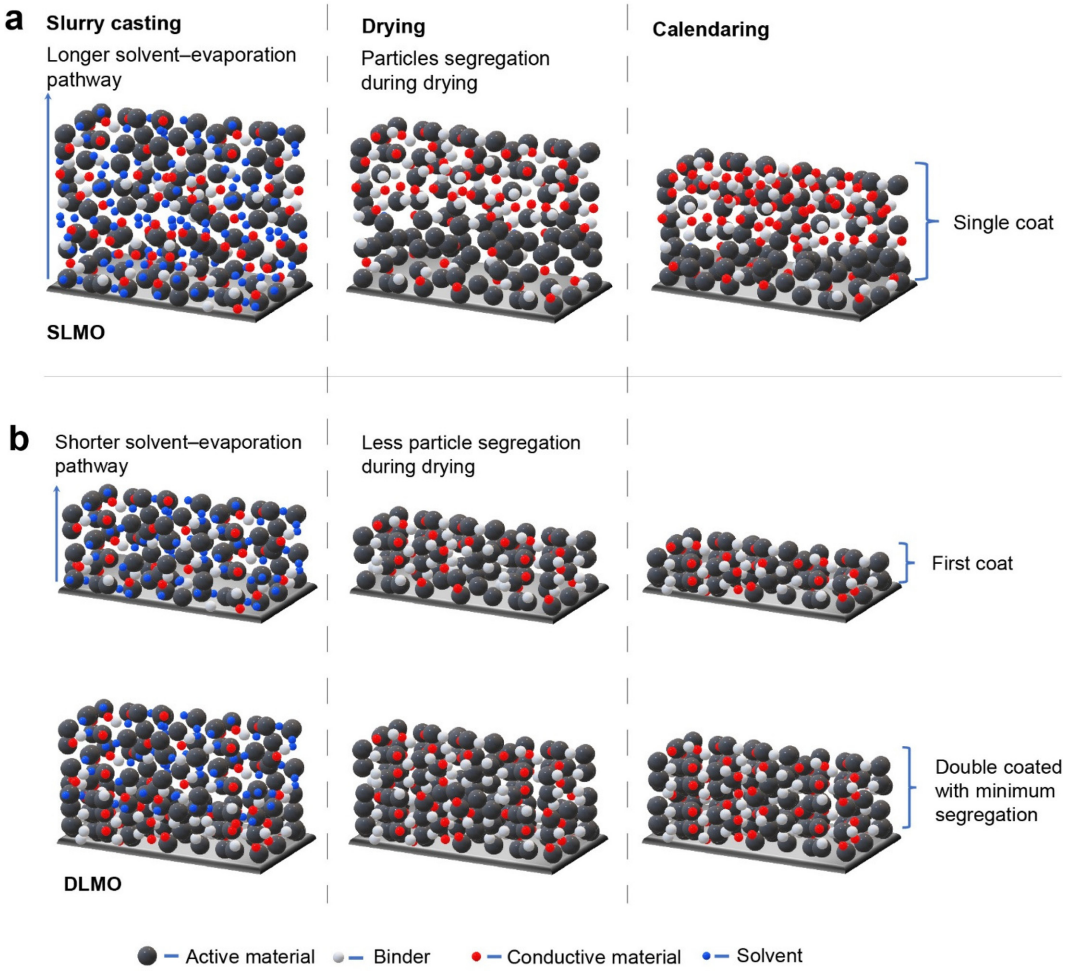

Fig. 3. Schematic of the electrode preparation steps for (a) SLMO and (b) DLMO

The changes in the physical state of the electrodes during the drying and calendaring processes are demonstrated in Fig. 3. In SLMO (Fig. 3a), extensive solvent evaporation during drying induces capillary forces that move the light electrode components such as polymeric binders and Super-P toward the top surface of the electrode. This causes particle agglomeration that results in the formation of a porous network of voids within the electrode and nonuniform component distribution. A uniform distribution of the conductive material is required to ensure high electrical conductivity because the specific electrical conductivity of a cathode active material is considerably low [24]. Moreover, high electrode density (mass loading per unit volume) is essential for the high electrochemical performance of electrodes. Owing to its compact morphological structure, uniform distribution of polymeric binders, and dense distribution of conductive C near the Al current collector, DLMO exhibited a lower sheet resistance (0.152 Ω cm^{-2}) than SLMO (0.177 Ω cm^{-2}) [25].

The distribution of electrode components, especially that of polymeric binders, affects the adhesion properties of electrodes. The formation of an intimate contact between electrodes and current collectors is important to achieve stable electrochemical properties [26-28]. The breakdown of the electrically conductive network among the active material, conductive carbon, and current collector in electrodes can lead to electrode failure [26]. Consequently, the adhesion properties of SLMO and DLMO were investigated using the SAICAS. SAICAS is better compared to the conventional peel test because it can determine adhesion properties at a specific depth by measuring both horizontal and vertical forces [29]. The fluctuations exhibited by the SLMO in the cutting mode and the unstable profile during the peeling mode (Fig. 4) is attributed to the uneven distribution of the binder and particle agglomeration leaving larger gaps and pores (corresponding to Fig. 2) [29]. The DLMO showed a more stable profile indicative of even particle distribution. Furthermore, the DLMO (74.7 N m^{-1}) exhibited higher adhesion strength than SLMO (57.8 N m^{-1}). The inferior adhesion properties of SLMO were attributed to the decreased distribution of polymeric binders on the Al-facing side of the electrode compared with that in DLMO, as seen in the cross-sectional SEM images (Fig. 2).

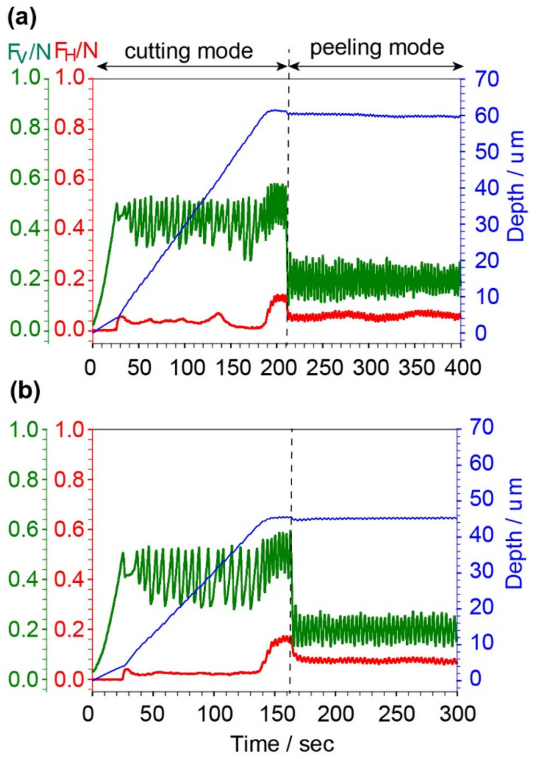

Fig. 4. SAICAS profiles for (a) SLMO and (b) DLMO

The morphology also affected the ionic conductivity of electrodes because the pores in the electrode serve as electrolyte reservoirs. The pore structure comprises connections between nodes (cavities) and ducts (throats); during wetting, the electrolyte fills the cavities first (converging) before spreading into the throats (diverging) [9,29]. The presence of large pores increases the convergence time, resulting in high electrolyte resistance and low electrode capacity [30]. To determine the effect of double coating on electrode stability, various electrochemical properties of SLMO and DLMO, such as cycling performance and rate capability, were investigated.

The voltage profiles of SLMO and DLMO during the last stabilization cycle are shown in Fig. 5a. Both SLMO and DLMO showed similar voltage profiles except for the discharge capacity. The dis-

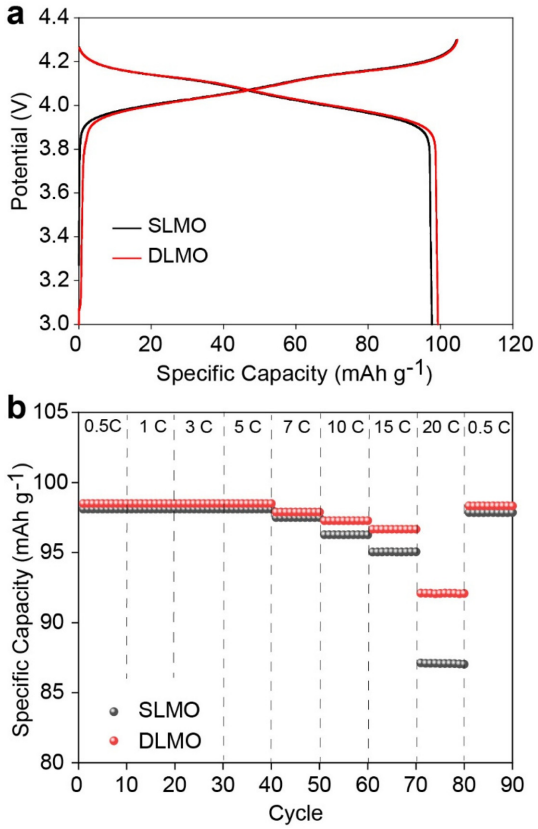

Fig. 5. (a) Charge/discharge profile curves and (b) rate capabilities for SLMO and DLMO.

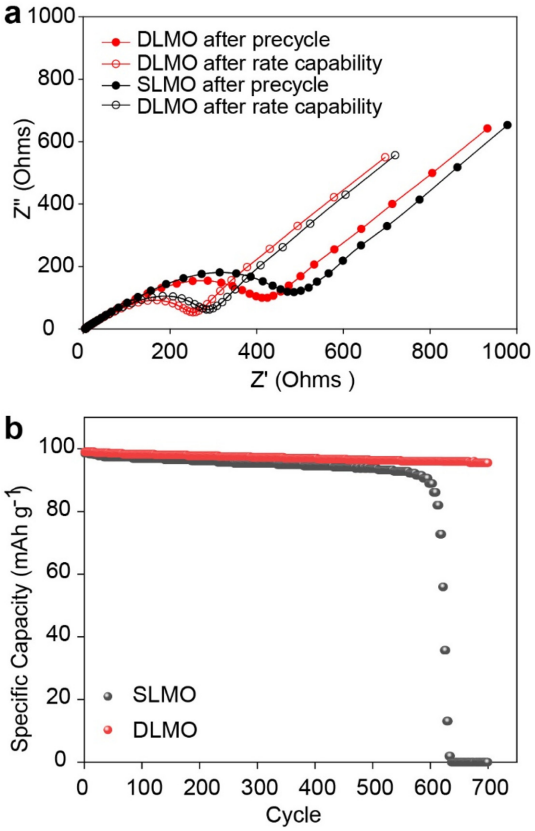

Fig. 6. (a) Nyquist plots and (b) long-term cycling performances of SLMO and DLMO.

charge capacity of DLMO (100.1 mAh g^{-1}) was 3.7% higher than that of SLMO (96.5 mAh g^{-1}) operated at C/5 (0.308 mA cm^{-2}).

The rate capabilities of SLMO and DLMO are shown in Fig. 5b. A significant difference in the rate performance of SLMO and DLMO is observed under high-C-rate discharging conditions (10, 15, and 20 C). For instance, at 20 C (30.8 mA cm^{-2}), the discharge capacity of DLMO (100.1 mAh g^{-1}) was 105% of that of SLMO (95.2 mAh g^{-1}). When the discharging current returned to C/2 (0.77 mA cm^{-2}) after 80 cycles, the initial discharge capacities of SLMO and DLMO were retained after the first cycle. This implied that the reduced discharge capacity of SLMO and DLMO under high-C-rate discharging conditions could be attributed to kinetic factors, regardless of active material damage and electrolyte consumption.

Furthermore, the electrochemical impedance of SLMO and DLMO was evaluated to elucidate the effects of double coating on rate capability. As shown in the Nyquist plots of SLMO and DLMO (Fig. 6a), the bulk resistance, which is associated with electrolyte infiltration into electrodes, was almost the same [31]. Nevertheless, DLMO exhibited a lower total resistance than SLMO. The impedance value in the medium to low-frequency range corresponded to resistance because of Li^+ ion migration through the electrode and the charge transfer resistance between the electrode and electrolyte. Thus, the low total resistance of DLMO could be attributed to the enhanced Li^+ ion migration. In contrast, the segregation of the binder and conductive materials to the surface of SLMO was considered as the main factor for the obstruction of the passage of Li^+ ions throughout the electrode

because the non-conductive PVDF binder blocked Li^+ ions [32-34]. Furthermore, the nonuniform pore size distribution caused by this segregation could lead to increased concentration gradients and induce polarization effects [35-37].

The cycling performances of SLMO and DLMO were investigated (Fig. 6b). The SLMO cell failed after around 605 cycles, whereat it exhibited a capacity retention of 80.8 mAh g^{-1} (87.8% of its initial discharge capacity) before it rapidly fell, whereas the DLMO cell continued to operate after 700 cycles, showing a capacity retention of 89.1 mAh g^{-1} (96.5% of its initial discharge capacity). As the cycling performance test proceeded, the liquid electrolyte was consumed on both the anode and cathode. This implied that the total resistance gradually increased with the cycle numbers during the test. The cells failed to exhibit the expected discharge capacity values when the total resistance of the cell exceeded the limiting values, leading to an IR drop during the test because the voltage of unit cells reached their cut-off values. As shown in the electrochemical impedance results, DLMO exhibited considerably lower total resistance than SLMO, which enabled the long-term maintenance of the cycling performance [33,38].

4. Conclusions

The effects of double-coated electrodes on electrochemical performance were investigated. Double coating was shown to facilitate the uniform distribution of particles in the slurry and the formation of small, uniformly distributed pores. The proposed method reduced the migration of low-density particles caused by capillary flow during drying. Further, the double-coated electrodes showed higher adhesion strength than the single-coated electrodes owing to uniform binder distribution. Moreover, the double-coated electrodes displayed higher performance at a high rate as well as long-term cyclability because of the improved electrode kinetics. The double-coated electrodes were also thinner than the single-coated electrodes under the same mass loading. This allowed for the production of high-density electrodes without excessive calendaring. The proposed method for electrode fabrication is effective and can be easily scaled up for the large-scale production of high-density electrodes.

Conflict of interest

The authors declare that they have no conflict of interest.

Acknowledgments

This research was supported by the National Research Foundation of Korea (NRF) funded by the Ministry of Science and ICT (NRF-2021R1|1A3059728). This research was also supported by Basic Science Research Program through the National Research Foundation of Korea (NRF) funded by the Ministry of Education (No.2018R1A6A1A03026005) and by the Technology Innovation Program (No. 20015759) funded by the Ministry of Trade, Industry & Energy (MOTIE, Korea). This results was supported by “Regional Innovation Strategy (RIS)” through the National Research Foundation of Korea (NRF) funded by the Ministry of Education (MOE) (2021RIS-004).

References

1. J. Zheng, M. H. Engelhard, D. Mei, S. Jiao, B. J. Polzin, J.-G. Zhang, and W. Xu, Electrolyte additive enabled fast charging and stable cycling lithium metal batteries, *Nat. Energy*, **2(3)**, 1-8, (2017).
2. J. Liu, Z. Bao, Y. Cui, E. J. Dufek, J. B. Goodenough, P. Khalifah, Q. Li, B. Y. Liaw, P. Liu, and A. Manthiram, Pathways for practical high-energy long-cycling lithium metal batteries, *Nat. Energy*, **4(3)**, 180-186, (2019).
3. R. Xu, X.-B. Cheng, C. Yan, X.-Q. Zhang, Y. Xiao, C.-Z. Zhao, J.-Q. Huang, and Q. Zhang, Artificial interphases for highly stable lithium metal anode, *Matter*, **1(2)**, 317-344, (2019).
4. M. H. Braga, N. S. Grundish, A. J. Murchison, and J. B. Goodenough, Alternative strategy for a safe rechargeable battery, *Energy Environm. Sci.*, **10(1)**, 331-336, (2017).
5. D. Jin, Y. Roh, T. Jo, M. H. Ryou, H. Lee, and Y. M. Lee, Robust cycling of ultrathin Li metal enabled by nitrate?preplanted Li powder composite, *Adv. Energy Mater.*, **11(18)**, 2003769, (2021).
6. S.-J. Cho, D.-E. Yu, T. P. Pollard, H. Moon, M. Jang, O. Borodin, and S.-Y. Lee, Nonflammable lithium metal full cells with ultra-high energy density based on coordinated carbonate electrolytes, *iScience*, **23(2)**, 100844, (2020).
7. R. E. Garcia, and Y.-M. Chiang, Spatially resolved mod-

eling of microstructurally complex battery architectures, *J. Electrochem. Soc.*, **154(9)**, A856, (2007).
8. V. Ramadesigan, P. W. Northrop, S. De, S. Santhanagopalan, R. D. Braatz, and V. R. Subramanian, Modeling and simulation of lithium-ion batteries from a systems engineering perspective, *J. Electrochem. Soc.*, **159(3)**, R31, (2012).
9. Y. Sheng, C. R. Fell, Y. K. Son, B. M. Metz, J. Jiang, and B. C. Church, Effect of calendering on electrode wettability in lithium-ion batteries, *Front. Energy Res.*, **2**, 56, (2014).
10. M. Singh, J. Kaiser, and H. Hahn, Thick electrodes for high energy lithium ion batteries, *J. Electrochem. Soc.*, **162(7)**, A1196, (2015).
11. M. Singh, J. Kaiser, and H. Hahn, A systematic study of thick electrodes for high energy lithium ion batteries, *J. Electroanal. Chem.*, **782**, 245-249, (2016).
12. Y. Kuang, C. Chen, D. Kirsch, and L. Hu, Thick electrode batteries: principles, opportunities, and challenges, *Adv. Energy Mater.*, **9(33)**, 1901457, (2019).
13. M. Baunach, S. Jaiser, S. Schmelzle, H. Nirschl, P. Scharfer, and W. Schabel, Delamination behavior of lithium-ion battery anodes: Influence of drying temperature during electrode processing, *Dry. Technol.*, **34(4)**, 462-473, (2016).
14. S. Jaiser, L. Funk, M. Baunach, P. Scharfer, and W. Schabel, Experimental investigation into battery electrode surfaces: The distribution of liquid at the surface and the emptying of pores during drying, *J. Colloid Interf. Sci.*, **494**, 22-31, (2017).
15. F. Huttner, W. Haselrieder, and A. Kwade, The influence of different post?drying procedures on remaining water content and physical and electrochemical properties of lithium?ion batteries, *Energy Technol.*, **8(2)**, 1900245, (2020).
16. J. Kumberg, W. Bauer, J. Schmatz, R. Diehm, M. Tönsmann, M. Müller, K. Ly, P. Scharfer, and W. Schabel, Reduced drying time of anodes for lithium?ion batteries through simultaneous multilayer coating, *Energy Technol.*, **9(10)**, 2100367, (2021).
17. M. Müller, L. Pfaffmann, S. Jaiser, M. Baunach, V. Trouillet, F. Scheiba, P. Scharfer, W. Schabel, and W. Bauer, Investigation of binder distribution in graphite anodes for lithium-ion batteries, *J. Power Sources*, **340**, 1-5, (2017).
18. B. G. Westphal, and A. Kwade, Critical electrode properties and drying conditions causing component segregation in graphitic anodes for lithium-ion batteries, *J. Energy Storage*, **18**, 509-517, (2018).
19. W. Wang, H. Qi, P. Liu, Y. Zhao, and H. Chang, Numerical simulation of densification of Cu–Al mixed metal powder during axial compaction, *Metals*, **8(7)**, 537, (2018).
20. H. Staf, P. Lindskog, D. C. Andersson, and P.-L. Larsson, On the influence of material parameters in a complex material model for powder compaction, *J. Mater. Eng. Perform.*, **25(10)**, 4408-4415, (2016).
21. L.-C. Chen, D. Liu, T.-J. Liu, C. Tiu, C.-R. Yang, W.-B. Chu, and C.-C. Wan, Improvement of lithium-ion battery performance using a two-layered cathode by simultaneous slot-die coating, *J. Energy Storage*, **5**, 156-162, (2016).
22. D. Liu, L. C. Chen, T. J. Liu, W. B. Chu, and C. Tiu, Improvement of lithium?ion battery performance by two?layered slot–die coating operation, *Energy Technol.*, **5(8)**, 1235-1241, (2017).
23. S. T. Taleghani, B. Marcos, K. Zaghib, and G. Lantagne, The effect of structural properties of a two-layered electrode on the Li-ion battery polarization, *J. Electrochem. Soc.*, **166(2)**, A225, (2019).
24. J. Ott, B. Völker, Y. Gan, R. M. McMeeking, and M. Kamlah, A micromechanical model for effective conductivity in granular electrode structures, *Acta Mech. Sin.*, **29(5)**, 682-698, (2013).
25. H. Bockholt, M. Indrikova, A. Netz, F. Golks, and A. Kwade, The interaction of consecutive process steps in the manufacturing of lithium-ion battery electrodes with regard to structural and electrochemical properties, *J. Power Sources*, **325**, 140-151, (2016).
26. T. Yoon, S. Park, J. Mun, J. H. Ryu, W. Choi, Y.-S. Kang, J.-H. Park, and S. M. Oh, Failure mechanisms of $LiNi_{0.5}Mn_{1.5}O_4$ electrode at elevated temperature, *J. Power Sources*, **215**, 312-316, (2012).
27. S. Choi, J. Kim, M. Eom, X. Meng, and D. Shin, Application of a carbon nanotube (CNT) sheet as a current collector for all-solid-state lithium batteries, *J. Power Sources*, **299**, 70-75, (2015).
28. J.-H. Kim, S. C. Woo, M.-S. Park, K. J. Kim, T. Yim, J.-S. Kim, and Y.-J. Kim, Capacity fading mechanism of $LiFePO_4$-based lithium secondary batteries for stationary energy storage, *J. Power Sources*, **229**, 190-197, (2013).
29. F. Durst, R. Haas, and W. Interthal, The nature of flows through porous media, *J. Non-Newton. Fluid Mech.*, **22(2)**, 169-189, (1987).
30. C. J. Bae, C. K. Erdonmez, J. W. Halloran, and Y. M. Chiang, Design of battery electrodes with dual?scale porosity to minimize tortuosity and maximize performance, *Adv. Mater.*, **25(9)**, 1254-1258, (2013).
31. B. Tran, I. O. Oladeji, Z. Wang, J. Calderon, G. Chai, D. Atherton, and L. Zhai, Adhesive PEG-based binder for aqueous fabrication of thick $Li_4Ti_5O_{12}$ electrode, *Electrochim. Acta*, **88**, 536-542, (2013).
32. G. Liu, H. Zheng, S. Kim, Y. Deng, A. Minor, X. Song, and V. Battaglia, Effects of various conductive additive and polymeric binder contents on the performance of a lithium-ion composite cathode, *J. Electrochem. Soc.*, **155(12)**, A887, (2008).
33. H. Zheng, L. Tan, G. Liu, X. Song, and V. S. Battaglia, Calendering effects on the physical and electrochemical properties of Li [Ni1/3Mn1/3Co1/3] O2 cathode, *J. Power Sources*, **208**, 52-57, (2012).
34. S. J. Babinec, H. Tang, G. Meyers, S. Hughes, and A.

Talik, Composite cathode structure/property relationships, *ECS Trans.*, **2(8)**, 93, (2007).
35. H. Dreger, W. Haselrieder, and A. Kwade, Influence of dispersing by extrusion and calendering on the performance of lithium-ion battery electrodes, *J. Energy Storage*, **21**, 231-240, (2019).
36. B. Vijayaraghavan, D. R. Ely, Y.-M. Chiang, R. García-García, and R. E. García, An analytical method to determine tortuosity in rechargeable battery electrodes, *J. Electrochem. Soc.*, **159(5)**, A548, (2012).
37. G. Sikha, B. N. Popov, and R. E. White, Effect of porosity on the capacity fade of a lithium-ion battery: Theory, *J. Electrochem. Soc.*, **151(7)**, A1104, (2004).
38. B. Son, M.-H. Ryou, J. Choi, S.-H. Kim, J. M. Ko, and Y. M. Lee, Effect of cathode/anode area ratio on electrochemical performance of lithium-ion batteries, *J. Power Sources*, **243**, 641-647, (2013).